# Enhancement of Hemodynamic Contrast in the Cancerous Breast by Carbogen Inspiration


Rabah Al abdi[1,4]; Harry L. Graber[1,2]; Christoph H. Schmitz[2,3]; Randall L. Barbour[1,2]

[1]SUNY Downstate Medical Center, Brooklyn, NY, USA; [2]NIRx Medizintechnik GmbH, Berlin, DEU;
[3]NIRx Medical Technologies, Glen Head, NY, USA; [4]Jordan University of Science and Technology, Irbid, JOR


**INTRODUCTION** Hallmarks of the tumor phenotype include increased stiffness [1], enhanced angiogenesis with sluggish perfusion [2], increased vascular leakiness leading to increased interstitial pressures [3], and increased metabolic demand [2]. Separately, it is known that the vascular autoregulation mechanism normally achieves a tight coupling between the vascular supply and prevailing metabolic demand, but that the fidelity of vascular autoregulation may be attenuated in tumor tissue as a consequence of alterations in the vascular endothelium and surrounding vascular smooth muscle [2]. One consequence of this is that many tumor types operate on the brink of hypoxemia, suggesting that the otherwise enhanced supply actually is limited, perhaps as a consequence of disturbances in hydrostatic pressures caused by vascular leakiness and changes to the interstitium scaffolding [1]. We hypothesized that manipulations of the oxygen supply-demand balance may produce responses that differ markedly between the tumor and surrounding healthy tissue. One approach that has recently been explored is the inspiration of carbogen [4]. While the carbogen response is tissue-specific, the most commonly seen response is vasodilation as a consequence of the effects of elevated $CO_2$ [4]. Here we use a recently developed an fNIRS-based breast imaging system [5] to explore the response of the healthy and tumor-bearing breast to a carbogen mixture consisting of 98% $O_2$ and 2% $CO_2$, as a basis for producing additional modulation of the oxygen supply-demand balance.

## INSTRUMENTATION

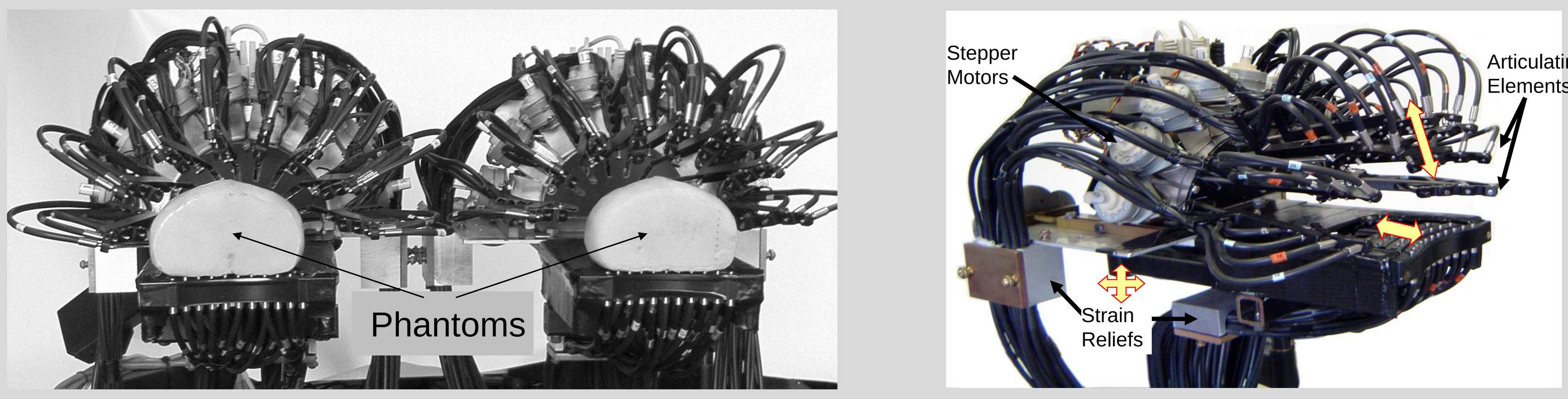


Fig. 1. Left: photograph of the sensing heads used for simultaneous dual-breast measurements, with breast-simulating phantoms in place. Right: side-view photograph of one of the left-breast sensing head.

## EXPERIMENTAL PROTOCOL

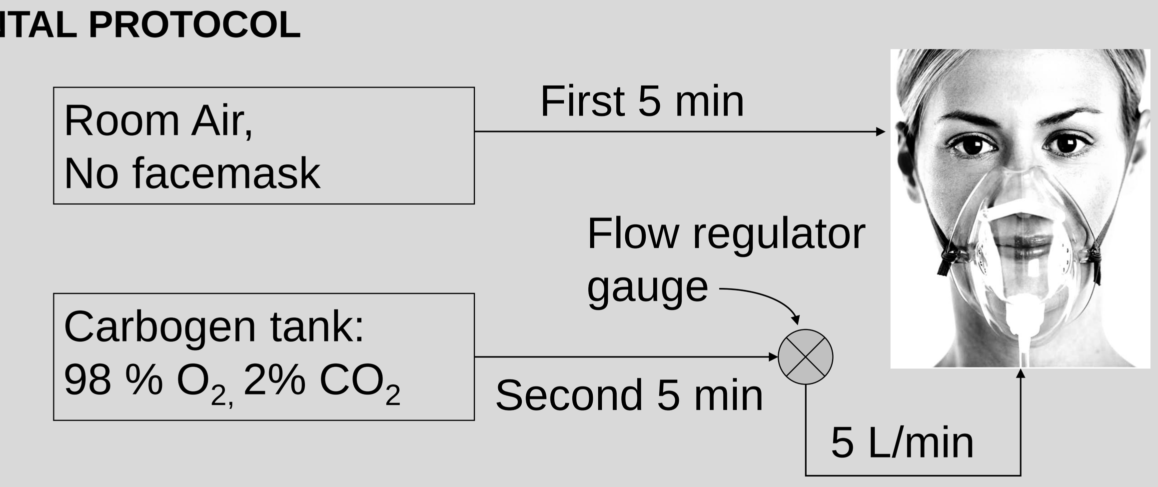


Fig. 2. Schematic depiction of the 10-minute experimental protocol.

Following a five-minute baseline scan, while breathing room air, a non-rebreathing facemask was applied and subjects breathed a modified carbogen mixture consisting of 98% $O_2$ and 2% $CO_2$ for an additional five minutes. Optical data were analyzed offline: application of a low-pass filter with a 0.2-Hz cutoff frequency was followed by use of the Normalized Difference Method to reconstruct images of oxygenated and deoxygenated hemoglobin (HbO, HbD), tissue oxygen saturation (HbSat), and blood volume (HbT) [6].

## STUDY POPULATION

| Category | Age (years) | BMI (kg/m²) |
|---|---|---|
| Active cancer (*n* = 16) | 50.8 ± 9.3 | 33.1 ± 7.8 |
| Benign pathologies (*n* = 18) | 48.2 ± 9.5 | 33.3 ± 6 |
| Healthy (*n* = 14) | 53.5 ± 11.5 | 32.6 ± 3.4 |

Table 1. Subjects' clinical information. Within the group of women who had active breast cancer at the time of examination, there were 10 with invasive ductal carcinoma, 2 with invasive mammary carcinoma, 1 with intraductal carcinoma, 1with invasive lobular carcinoma, 1 with ductal carcinoma *in situ* (DCIS), and 1 with invasive mucinous carcinoma in addition to extensive DCIS. Tumor dimensions ranged from 0.5 cm to 5 cm.

## INDIVIDUAL Hb SIGNAL COMPONENT RESULTS

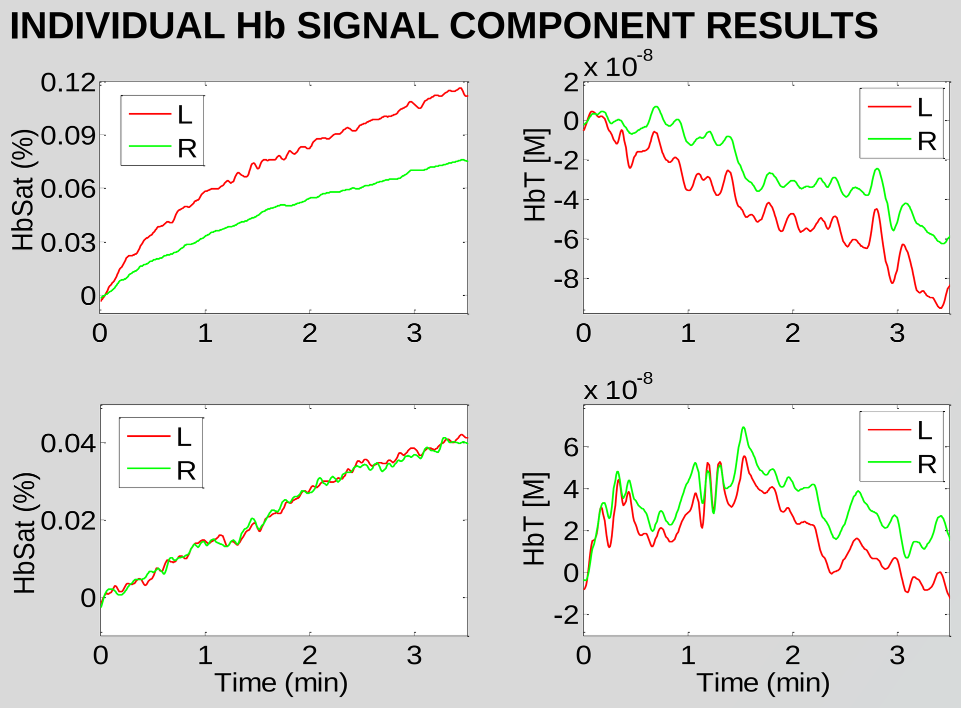

Fig. 4. Representative volume-averaged HbSat (left) and HbT (right) time series, during the course of carbogen inhalation. Top: subject is 41 y/o with BMI = 27, and has a 2-cm intra-lobular carcinoma in the left breast. Bottom: healthy subject, 43 y/o with BMI = 35.

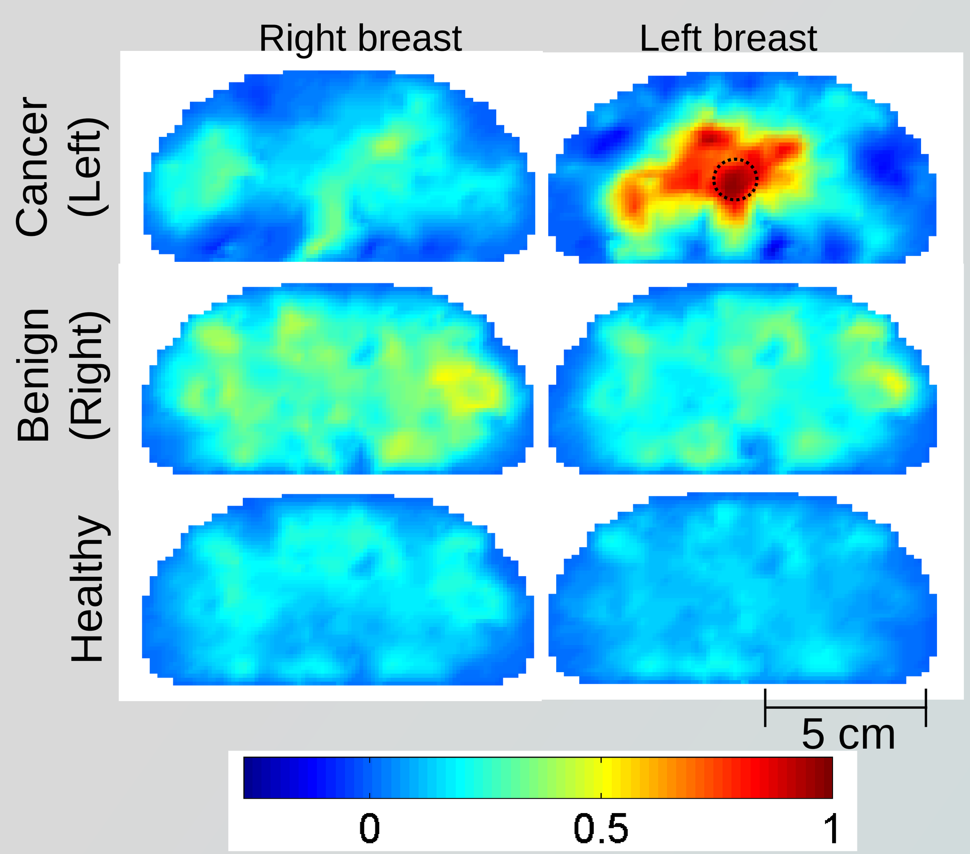


Fig. 5. Coronal sections of 3D reconstructed images of HbSat, at a time frame near the end of the carbogen-inspiration period. The numerical (i.e., color) scale for all images is normalized to the maximum absolute value across subjects. Dotted black circle indicates the size and location the tumor, when present, as determined from surgical and conventional imaging procedures. Breast-cancer subject is 41 y/o with BMI = 27 and has a 2-cm intra-lobular carcinoma in the left breast. Benign-pathology subject is 48 y/o with BMI = 46 and has fibrocystic changes in the right breast. Healthy control subject is 43 y/o with BMI = 35.

## INDIVIDUAL Hb SIGNAL COMPONENT RESULTS (cont.)

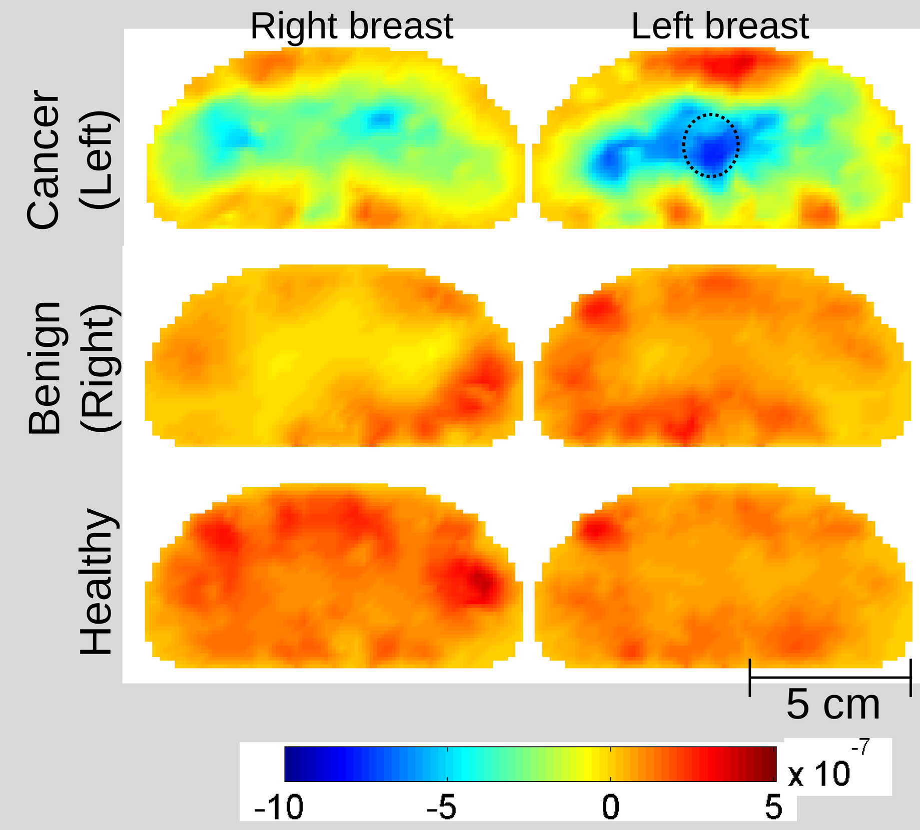


Fig. 6. Coronal sections of 3D reconstructed images of HbT. Study participants and image time frame are the same as those considered in Fig. 5 ; dotted black circle indicates the size and location the tumor, when present. In this case, however, the numerical (i.e., color) scale is the recovered range of HbT concentrations (moles-liter$^{-1}$), referenced to a baseline-mean value derived from data collected prior to the start of carbogen inspiration. (Thus negative concentration values are seen in places where HbT has decreased in comparison to the pre-carbogen time interval.) Strong qualitative similarity between image features in Figs. 5 and 6 is a factor that suggested the idea of combining multiple Hb-signal components into a single index, with the goal of improving the image spatial resolution and contrast.

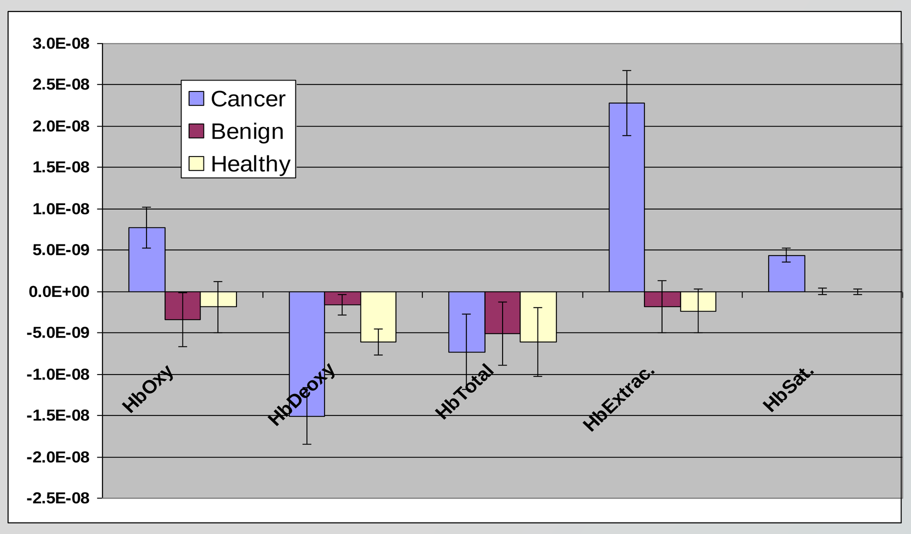


Fig. 7. Group paired-difference means (colored bar heights) and standard errors (error bars), computed from spatial mean values of reconstructed images of HbO, HbD, HbT, Hb $O_2$ Extraction (i.e., HbO – HbD), and HbSat. (For display purposes, HbSat is scaled by $10^{-7}$.) As in Figs. 5 and 6, image values are referenced to the corresponding baseline mean value. Thus a negative value on the vertical axis indicates that the inter-breast difference is lower after carbogen inspiration than before. For cancer and benign-pathology groups, difference is computed as affected-minus-unaffected breast; for healthy controls, as left-minus-right breast. Statistically significant differences (p<0.01) between the cancer group and both the healthy and the benign-pathology are found for components Hb except HbT.

| Hb-Signal Component | AUC | p-value |
|---|---|---|
| HbO | 0.693 | 0.021 |
| HbD | 0.766 | 0.001 |
| HbT | 0.522 | 0.792 |
| Extraction | 0.844 | 0.000 |
| HbSat | 0.873 | 0.000 |

Table 2. Receiver operator characteristic analysis [7] for the same spatial-means of paired difference data considered in Fig. 7. The AUC (i.e., area under the curve) metric is the percentage of subjects who are correctly identified as belonging to either the cancer or "other" (i.e., having either a benign pathology or none) group, in paired comparisons between one randomly chosen member from each group. All Hb-signal components except for HbT are statistically significant breast-cancer diagnostics indicators at the individual-subject level.

## MAHALANOBIS DISTANCE-BASED RESULTS

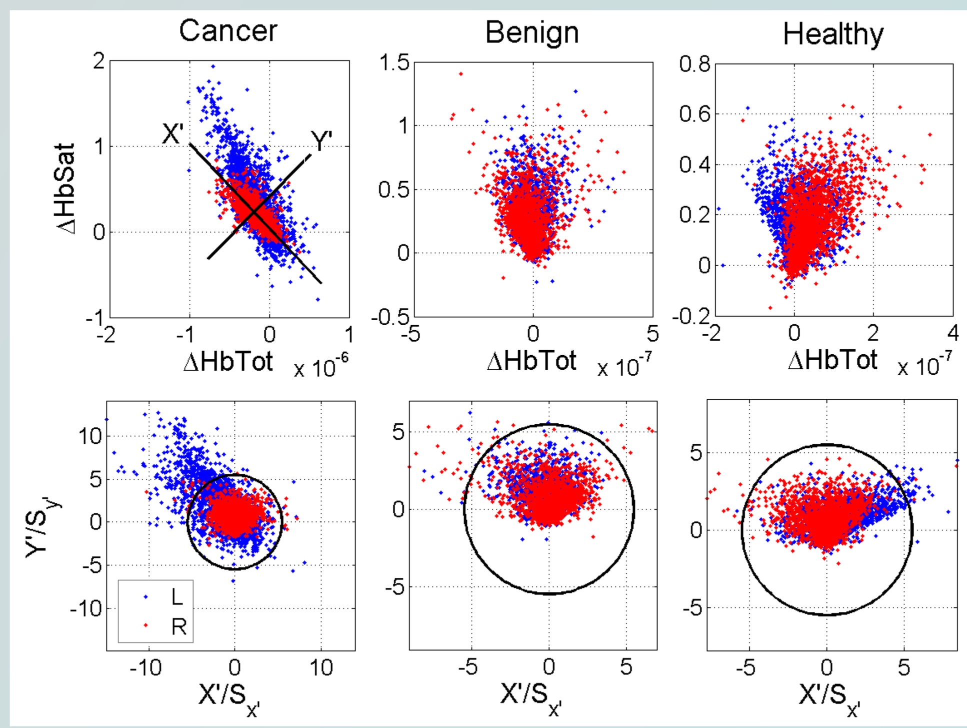


Fig. 8: Computation of the inter-breast Mahalanobis distance (MD) [8]. (a) Scatterplots (each dot represents one image pixel) of two Hb-signal components (HbSat and HbT in these examples) reveal that they tend to co-vary. Thus we seek to incorporate both of them into a single index. (b) In this rotated and rescaled representation of the scatterplots, the MD for each data point is the distance from the point to the origin.

Empirically, we find that approximately 1% of data points have MD > 5.5 (black circles in (b)), for both healthy and affected breasts. But for cancer subjects, the inter-breast contrast is substantially increased when we modify the MD computation by referencing the data for one breast to the mean and covariance estimates for the contralateral breast, as indicated in the following formula:

$$MD_{breast1} = \sqrt{\left(x_{breast1} - \bar{x}_{breast2}\right)^{T} \left(\mathbf{C}_{breast2}\right)^{-1} \left(x_{breast1} - \bar{x}_{breast2}\right)} \qquad (1)$$

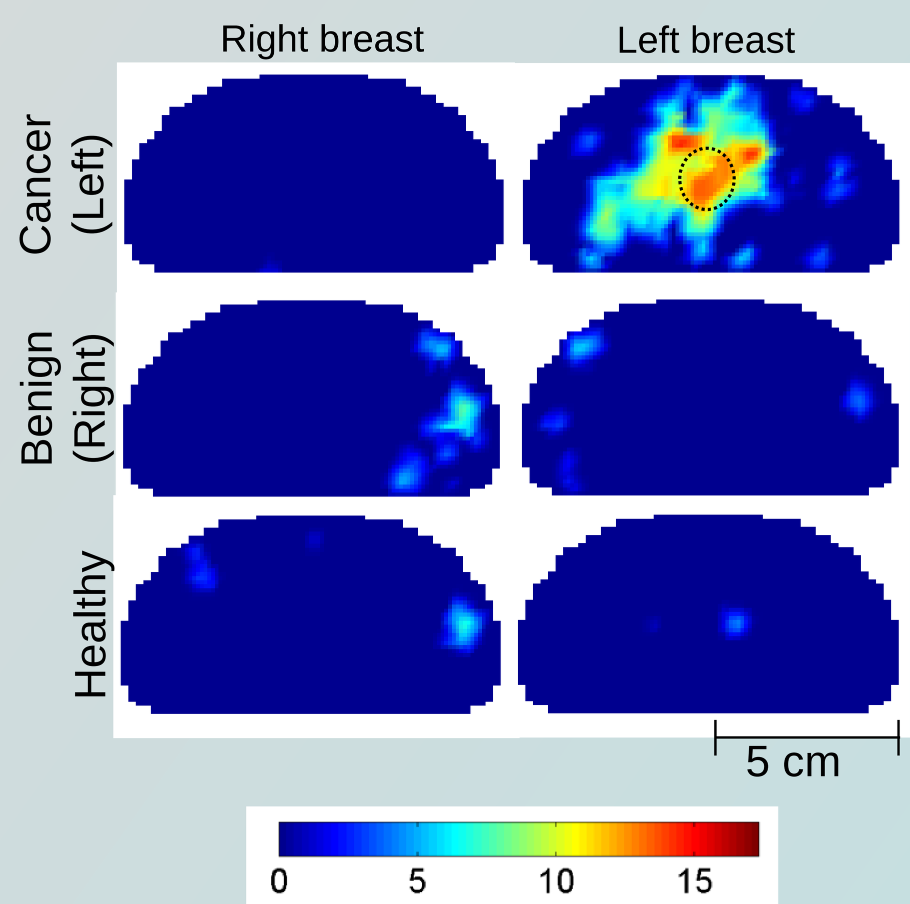


Fig. 9. Coronal sections of 3D spatial maps of the MD calculated using Eq. (1). To emphasize large-MD features, images are thresholded to show only regions with MD > 5.5. While similar results are obtained for all pairings of Hb-signal components, the images shown are MDs derived from the (HbT,HbSat) pair. Study participants and image time frame are the same as those considered in Figs. 5 and 6; dotted black circle indicates the size and location the tumor, when present. In comparison to the individual-component image data, the additional operations performed have the effect of enhancing image contrast.

| Comparison: Cancer vs. | AUC (%) | Sensitivity (%) [95% CL (%)] | Specificity (%) [95% CL (%)] |
|---|---|---|---|
| 1) Healthy controls | 92 | 100 [76 – 100] | 71 [42 – 90] |
| 2) Benign pathologies | 88 | 100 [76 – 100] | 78 [52 – 93] |
| (1) and (2) | 90 | 100 [76 – 100] | 75 [56 – 88] |

Table 3. Group-level diagnostic accuracy achievable using the inter-breast paired difference between numbers of image pixels with MD > 5.5 as the predictor

## CONCLUSION

Results presented show that the implemented carbogen inspiration protocol can improve image contrast between breast tumors and both the surrounding healthy tissue and the contralateral breast. The markedly different responses between tumor and non-tumor tissues plausibly is a reflection of differences in oxygen supply-demand balance.


**References**

[1] S. Kumar and V. M. Weaver, *Cancer Metastasis Rev.* **28**, 113-127 (2009).
[2] P. Vaupel et al., *Cancer Res.* **49**, 6449-6465 (1989).
[3] R.E. Hendrick, *Breast MRI: Fundamentals and Technical Aspects* (Springer, 2008), Chap. 8.
[4] C. M. Carpenter et al., *J. Biomedical Optics* **15**, 036026 (2010).
[5] R. Al abdi et al., *J. Optical Society of America A* **28**, 2473-2493 (2011).
[6] Y. Pei *et al.*, *Applied Optics* **40**, 5755-5769 (2001).
[8] R. De Measschalck *et al.*, *Chemometrics and Intelligent Laboratory Systems* **50**, 1-18 (2000).
[7] C.E. Metz, *Seminars in Nuclear Medicine* **8**, 283-298 (1978)



**Acknowledgements**

This research was supported by the National Institutes of Health (NIH) grant R41CA096102, the U.S. Army grant DAMD017-03-C-0018, the Susan G. Komen Foundation, the New York State Department of Health (Empire Clinical Research Investigator Program), and by the New York State Foundation for Science, Technology and Innovation-Technology Transfer Incentive Program (NYSTAR-TIPP) grant C020041.